Heliyon 7 (2021) e06984

Contents lists available at ScienceDirect

Heliyon

journal homepage: www.cell.com/heliyon

Research article

Photocatalytic degradation of nitrobenzene in wastewater by persulfate integrated with Ag/Pb_3O_4 semiconductor under visible light irradiation

Wen-Shing Chen *, Yi-Chen Liu

Department of Chemical and Materials Engineering, National Yunlin University of Science & Technology, 123 University Road, Section 3, Douliou, Yunlin 640, Taiwan

ARTICLE INFO

Keywords:
Nitrobenzene
Persulfate
Ag/Pb_3O_4 semiconductor
Sulfate radical

ABSTRACT

Nitrobenzene oxidation was executed utilizing an innovative method, in which Ag/Pb_3O_4 semiconductors irradiated by visible light were used for activation of persulfate into sulfate radicals. Batch mode experiments were accomplished to elucidate the effect of persulfate concentrations and Ag/Pb_3O_4 dosages on the nitrobenzene oxidation behaviors. The physicochemical properties of original and reacted Ag/Pb_3O_4 were illustrated by X-ray diffraction analyses, UV-Vis diffuse reflectance spectra, FE-SEM images, EDS analyses, photoluminescence spectra and X-ray photoelectron spectra, respectively. The main oxidant was hypothesized to be sulfate radicals, induced from persulfate caused by photocatalysis of Ag/Pb_3O_4. It was clearly reflected on the scavenging experiments with addition of benzene, ethanol and methanol individually. As far as degradation pathways concerned, nitrobenzene was essentially transformed into hydroxycyclohexadienyl radicals, and sequentially converted to 2-nitrophenol, 3-nitrophenol or 4-nitrophenol simultaneously. Denitration of nitrophenols gave rise to synthesis of phenol, followed with generation of hydroquinone and *p*-benzoquinone.

1. Introduction

Nitrobenzene is a highly important raw chemical for manufacture of polyurethane via intermediate formation of aniline. Its derivatives have been broadly used for production of pesticides, explosives, plastics and pharmaceuticals (Weissermel and Arpe, 1991). Because of serious risks for inherent mutagenicity and carcinogenicity, wastewater polluted with nitrobenzene and its derivatives would bring about great impact on the water bodies and soil environment (Holder, 1999; Wang et al., 2011). Therefore, effective treating manners for industrial effluent have received much attention and been developed.

Because of resistance to biodegradation caused by the electron-withdrawing effect of nitro groups, advanced oxidation techniques have been wildly investigated for nitrobenzene removal in wastewater (Zhu et al., 2007; Sun et al., 2019). As far as titanium dioxide photocatalyst is concerned, the nitrobenzene removal rate could be obviously enhanced by means of impregnation of Li_2O or Fe_2O_3, which successfully inhibits recombination of photogenerated electrons and holes (Nitoi et al., 2015). On the other hand, TiO_2 absorbance band was effectively shifted to the visible light range on account of doping ammonium nitrate and cerium nitrate (Shen et al., 2009; Tayade et al., 2011). Besides, ozone assisted with ultrasound was applied for oxidation of nitrobenzene. The hydroxyl radicals appear to be main oxidizing agents (Weavers et al., 1998; Zhao et al., 2015). Ozone catalyzed with honeycomb (Al_2O_3-SiO_2) or ZSM-5 has been extensively studied for treatment of wastewater contaminated with nitrobenzene (Zhao et al., 2008, 2009; Chen et al., 2018). In another aspect, nitrobenzene decomposition rates were drastically increased using an electrochemical process, wherein TiO_2 nanotubes were incorporated into PbO_2 electrode plates, leading to ordered structure and higher specific surface areas (Chen et al., 2014; Xia et al., 2014; Gu et al., 2018). The hydroxyl radical-based Fenton manners have been also investigated, including Fenton's reagents (Carlos et al., 2010; Jiang et al., 2011; Zhang et al., 2014), Fenton-like reagents (Nichela et al., 2013; Duan et al., 2016; Sun et al., 2019), ultrasound-assisted Fenton (Elshafei et al., 2014) and fluidization-Fenton process (Anotai et al., 2009; Ratanatamskul et al., 2010).

Up to now, tremendous efforts have been devoted to mineralization of nitrobenzene in wastewater with sulfate radical related processes. Persulfate activated with thermal energy has been applied for oxidation of nitrobenzene, of which degradation intermediates include 2-nitrophenol, 4-nitrophenol, 2,4-dinitrophenol and 2,6-dinitrophenol (Ji et al., 2017). Besides, persulfate assisted with ozone could significantly enhance

* Corresponding author.
E-mail address: chenwen@yuntech.edu.tw (W.-S. Chen).

https://doi.org/10.1016/j.heliyon.2021.e06984
Received 4 February 2021; Received in revised form 10 February 2021; Accepted 29 April 2021

sulfate radical yields (Qiao et al., 2019). For the sake of accelerating nitrobenzene removal, persulfate anions could be effectively transformed into sulfate radicals by means of activation with zero-valent Zn^0 (Guo et al., 2017) or magnetized Fe^0 (Pan et al., 2017; Zhang et al., 2019). Persulfate anions activated by ultra-violet light were also used for mineralization of nitrobenzene (De Luca et al., 2017). Nonetheless, semiconductor activation of persulfate under visible light irradiation has been scarcely investigated for oxidation of nitrobenzene. The luminous energy of visible light, corresponding to the band gap energy of semiconductors, could excite them to generate electron-hole pairs. Persulfate anions activated with photogenerated electrons may be converted into sulfate radicals (Chen and Shih, 2020).

In this study, an innovative manner for nitrobenzene elimination in aqueous phase would be established. Sulfate radicals were expected to be generated from persulfate anions via activation of Ag/Pb_3O_4 irradiated with visible light, recognized as semiconductors (Mukhopadhyay et al., 1997; Terpstra et al., 1997; Mohammadikish and Zamani, 2018). The effects of operating variables on the nitrobenzene removal performance were investigated, including persulfate concentrations and Ag/Pb_3O_4 dosages. Additionally, nitrobenzene degradation pathways imposed by the persulfate coupled with Ag/Pb_3O_4 semiconductors under visible light irradiation were also presented.

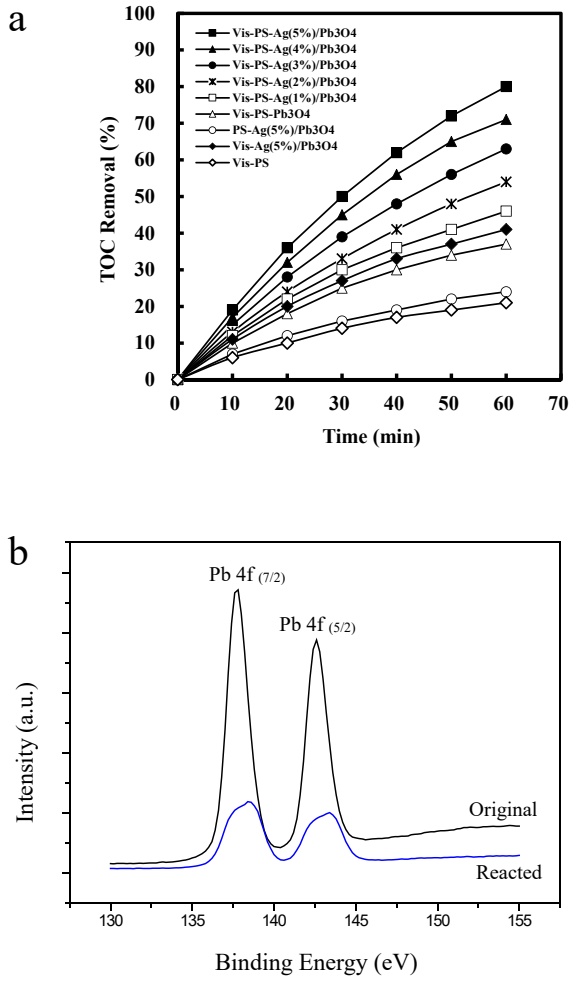

Figure 1. a Time-dependent modes of TOC removal percentages by Persulfate, Pb_3O_4, Ag (1wt%)/Pb_3O_4, Ag (2wt%)/Pb_3O_4, Ag (3wt%)/Pb_3O_4, Ag (4wt %)/Pb_3O_4 and Ag (5wt%)/Pb_3O_4, respectively under the conditions of visible light power = 103.2 W, T = 318 K, persulfate concentration = 100 mM and Ag/Pb_3O_4 dosage = 1.5 g L^{-1}. b X-ray photoelectron spectra of Pb 4f core level for original Ag (5wt%)/Pb_3O_4 and reacted Ag (5wt%)/Pb_3O_4 semiconductors.

2. Experimental methods

2.1. Testing of persulfate integrated with Ag/Pb_3O_4 under visible light irradiation

Experimental system accompanied with chief apparatus was consulted with our previous work (Chen and Huang, 2020). The photocatalytic reactor was a quartz cylinder equipped with internal cooling coils and a magnetic stirrer, wherein temperature was adjusted through a thermostat (VWR Scientific Products Corp. 1167 Model). Visible light was emitted along the surrounding by twelve lamps (8.6 W each) with low-pressure mercury vapor at the wavelength peaks of 438 nm, 550 nm and 619 nm (Philips Corp. PL-S Lamps). The synthesized feedstock at 1.0 mM concentrations of nitrobenzene (≥99.9%, Riedel-de Haen), was consistent with real concentrations of industrial wastewater (He et al., 2009). Prior to tests, it was well blended with proportional amounts of sodium persulfate (≥99.5%, Fluka). The Ag/Pb_3O_4, prepared from Pb_3O_4 powder (99.9%, Sigma-Aldrich) impregnated by incipient wetness with 1–5 wt% of silver nitrate (≥99.5%, Riedel-de Haen), respectively and following calcination at 823 K for 3 h with 400 mesh sieving (Satdeve et al., 2019), was packed into the basket, installed between the photocatalytic reactor center and walls. Within the period of tests, wastewater was sampled from the reactor under an identical time interval, then immediately quenched to the temperature of 273 ± 0.5 K to end oxidation reaction (Chen and Huang, 2015). Samples were imposed on total organic carbon (TOC) analyses for evaluation of organic compound content. The Ag/Pb_3O_4 retrieved from oxidation tests would execute X-ray photoelectron spectroscopy (XPS). In this research, experiments were carried out batch-wisely under a series of persulfate anion concentrations (80.0–140.0 mM). Further photocatalytic tests were undertaken with diverse Ag/Pb_3O_4 dosages (1.2 up to 2.1 g L^{-1}) for promotion of nitrobenzene removal rates. All experiments were undergone to the least extent for confirmation of data.

2.2. Total organic carbon (TOC) analysis

Within the period of tests for persulfate coupled with Ag/Pb_3O_4 under visible light irradiation, samples were periodically taken and directly analyzed using a TOC instrument (GE Corp. Sievers InnovOx). The hydrocarbons contained would be quantified by means of nondispersive infrared (NDIR) analyses on carbon dioxide generated from persulfate oxidation assisted with supercritical water conditions. In contrast, non-hydrocarbons were transformed into carbonic acid. TOC concentrations reported were founded on the calibration curve, established cautiously among the range (0–4.0 mM) using potassium hydrogen phthalate standard solutions.

2.3. Physicochemical properties of Ag/Pb_3O_4

The crystalline structures of original Ag/Pb_3O_4 semiconductors were determined by a X-ray diffractometer (Brucker, Advance-D825A) equipped with monochromated high-intensity CuKα radiation (λ = 1.5418 Å) under the accelerating voltage of 40 kV and emission current of 30 mA at the 2θ range of 10–80°. With regard to light absorption band of Ag/Pb_3O_4, the Ultraviolet-Visible diffuse reflectance spectra were examined by means of an UV-Vis spectrometer (PerkinElmer Corp. Lambda 850 Model). The UV-DRS obtained were among the wavelength range of 400–800 nm on the basis of $BaSO_4$ reference. According to scanning operated in a field-emission scanning electron microscope (FE-SEM, JSM-6500F, JEOL) fitted with an energy dispersive X-ray spectroscope (EDS, JED-2300, JEOL), Ag/Pb_3O_4 semiconductors were inspected for their surface morphology and silver extents impregnated. The photoluminescence spectra of the samples were monitored using a fluorescence spectrophotometer, with an excitation wavelength of 325 nm, fitted with a detector of charge couple device (Hitachi, F-4500). On the other hand, XPS profiles given from a X-ray photoelectron

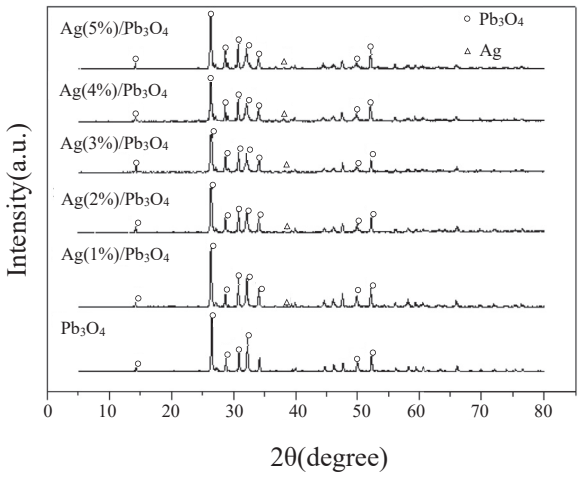

Figure 2. The XRD patterns of Pb_3O_4 and Ag/Pb_3O_4 semiconductors.

spectrometer integrated with a monochromatic AlKα source (Kratos Analytical Ltd. Axis Ultra) were utilized for elucidation of electronic states on original and reacted Ag/Pb_3O_4 semiconductors. The C 1s core level at 284.8 eV of adventitious carbon was employed as standard binding energy.

Table 1. The band gap energy of Ag/Pb_3O_4 semiconductors determined by UV-DRS.

Semiconductors	Band gap energy (eV)
Pb_3O_4	2.20
Ag (1wt%)/Pb_3O_4	2.10
Ag (2wt%)/Pb_3O_4	2.01
Ag (3wt%)/Pb_3O_4	1.91
Ag (4wt%)/Pb_3O_4	1.82
Ag (5wt%)/Pb_3O_4	1.72

2.4. Gas chromatography-mass spectrometry analysis (GC-MS)

Until 30 min reaction for persulfate integrated with Ag/Pb_3O_4 under visible light irradiation, wastewater (300 mL) was sampled from the photocatalytic reactor. The aqueous solution was agitated with micro-extraction fiber coated with Carboxen/Polydimethylsiloxane (Supelco.) for extraction of oxidative degradation intermediates. Sequentially, the fiber was packed into a micro-needle and transferred to an injection port

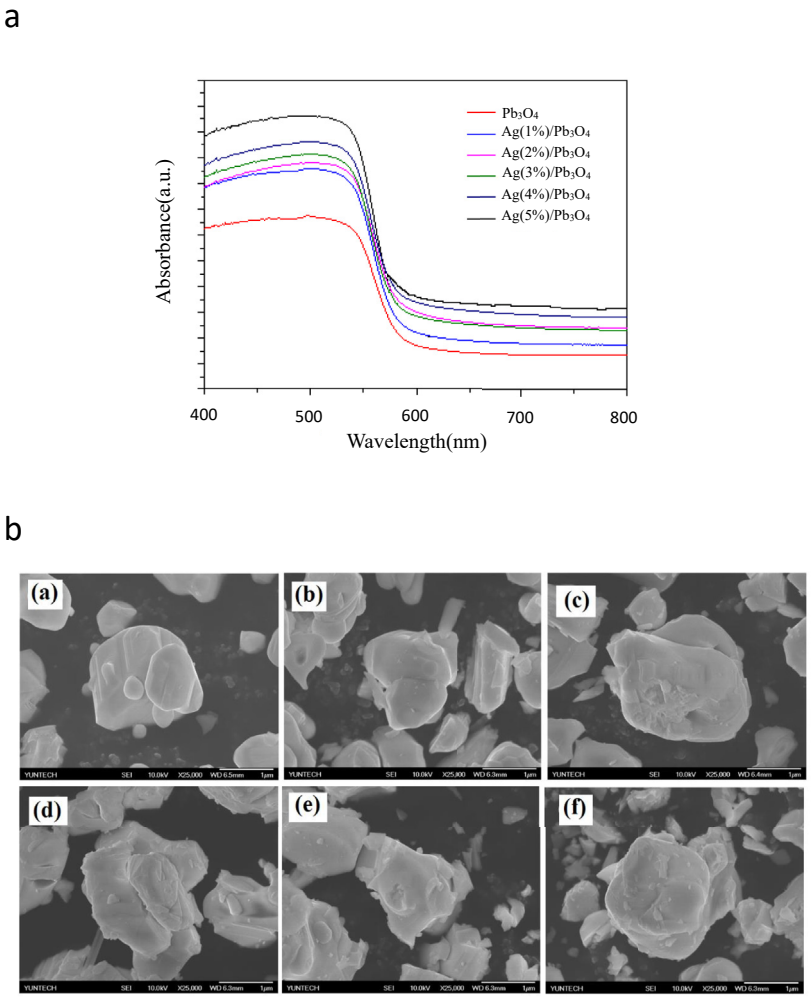

Figure 3. a UV-vis diffuse reflectance spectra of Pb_3O_4, Ag (1wt%)/Pb_3O_4, Ag (2wt%)/Pb_3O_4, Ag (3wt%)/Pb_3O_4, Ag (4wt%)/Pb_3O_4 and Ag (5wt%)/Pb_3O_4 semiconductors. b FE-SEM images of the (a) Pb_3O_4, (b) Ag (1wt%)/Pb_3O_4, (c) Ag (2wt%)/Pb_3O_4, (d) Ag (3wt%)/Pb_3O_4, (e) Ag (4wt%)/Pb_3O_4 and (f) Ag (5wt%)/Pb_3O_4 semiconductors.

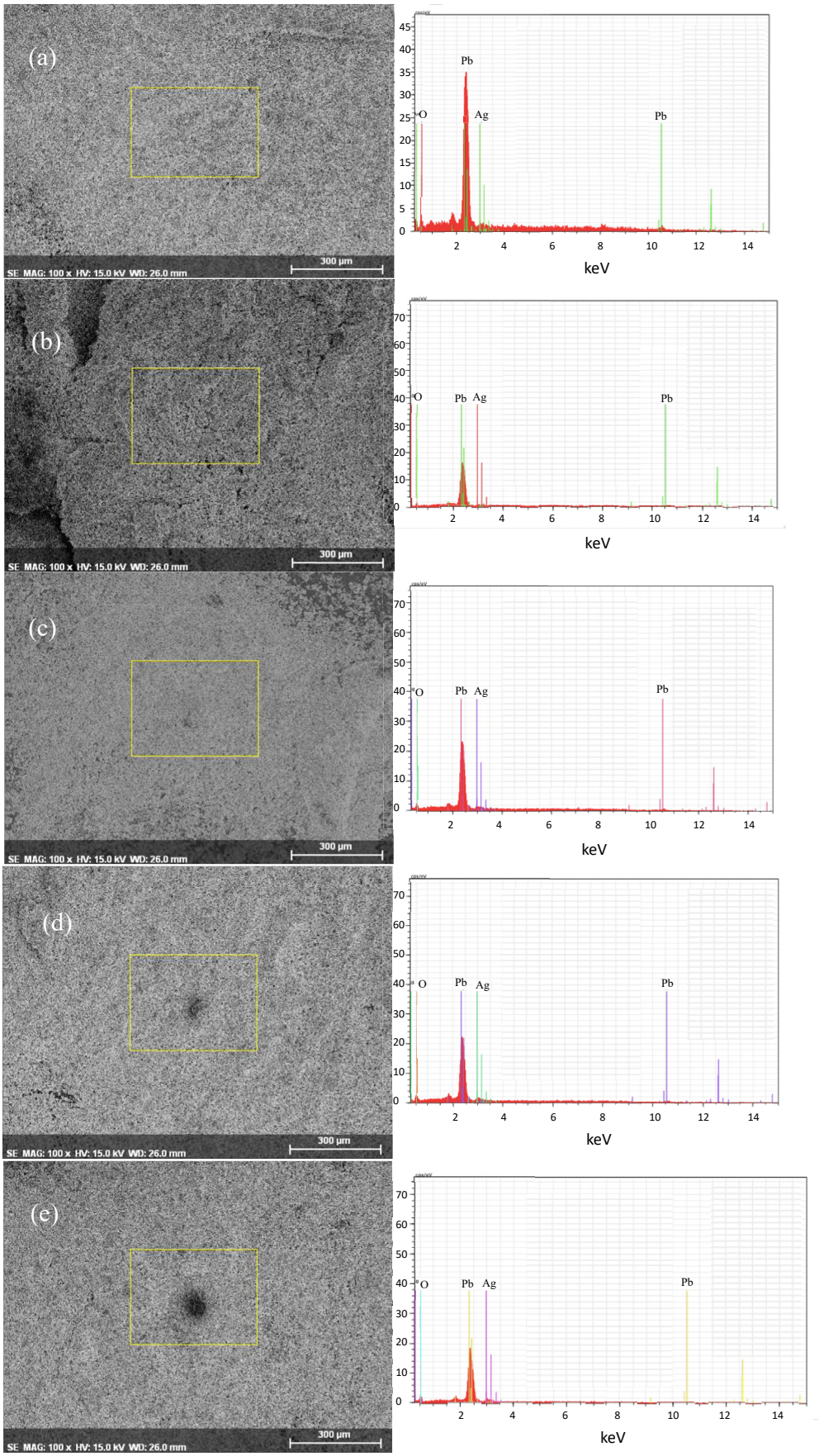

Figure 4. The EDS element analyses on Ag/Pb_3O_4 semiconductors: (a) Ag (1wt%)/Pb_3O_4, (b) Ag (2wt%)/Pb_3O_4, (c) Ag (3wt%)/Pb_3O_4, (d) Ag (4wt%)/Pb_3O_4 and (e) Ag (5wt%)/Pb_3O_4.

Table 2. The EDS element analyses on Ag/Pb_3O_4 semiconductors.

Semiconductor	Pb (wt%)	O (wt%)	Ag (wt%)
Pb_3O_4	52.46	47.54	0
Ag (1wt%)/Pb_3O_4	49.30	49.91	0.79
Ag (2wt%)/Pb_3O_4	48.40	49.82	1.78
Ag (3wt%)/Pb_3O_4	50.31	46.90	2.79
Ag (4wt%)/Pb_3O_4	41.04	55.28	3.68
Ag (5wt%)/Pb_3O_4	41.56	53.64	4.80

on the front of gas chromatograph−mass spectrometer (Hewlett Packard 59864B/HP 5973 MASS). Helium gas was utilized as carrier gas and an analytic capillary column was installed with dimensions of 30 m × 0.25 mm (Metal ULTRA ALLOY UA-5). According to the mass spectra procured with reference to those of standards, the major degradation intermediates of nitrobenzene were confidently resolved.

2.5. Scavenging effects

Upon addition of diverse scavengers, including benzene, methanol and ethanol respectively, mineralization of nitrobenzene by persulfate integrated with Ag/Pb_3O_4 under visible light irradiation was performed for elucidation of chief oxidizing agents (Liang and Su, 2009; Lin et al., 2013). The nitrobenzene removal percentage was directly monitored through the peak at 262 nm shown on an UV-Vis spectrophotometer (PerkinElmer Inc. Lambda 850) (Nichela et al., 2013). During the pretests, benzene has been shown to be most serious scavengers. As far as assessments of sulfate radical yields under various operating conditions were concerned, appropriate amounts of benzene scavenger accompanied with nitrobenzene were added to wastewater simultaneously to present the decrement of nitrobenzene removal percentage. Thus, the benzene scavenging effect may substitute for sulfate radical yields in this work.

3. Results and discussion

3.1. Comparison of persulfate oxidation and persulfate integrated with Ag/Pb_3O_4 under visible light irradiation

Figure 1a illustrates the time-flow modes of TOC removal percentages executed by persulfate oxidation and persulfate integrated with Ag/Pb_3O_4 irradiated with visible light, respectively. Transparently, nitrobenzene removal percentages resulted from persulfate integrated with Ag/Pb_3O_4 method were much higher than those utilizing persulfate oxidation alone and persulfate integrated with Pb_3O_4 process. Additionally, Ag (5%)/Pb_3O_4 combined with persulfate exhibited synergistic performance as compared with photocatalytic behaviors by the Ag (5%)/Pb_3O_4 and persulfate, individually. This phenomenon may be attributed to enhancement on sulfate radical yields. It has been reported that persulfate anions could be successfully converted into sulfate radicals by activation with photocatalysis of Ag/Pb_3O_4 semiconductors (Sakthivel et al., 2019). Besides, Ag metal was admitted to serve as an electron sink and reinforced charge separation, resulting in prevention from recombination of photogenerated electrons and holes on the surface of Pb_3O_4 (Han et al., 2012; Zhang et al., 2017). The reactions inferred are shown as follows.

$$Ag/Pb_3O_4 + h\nu \rightarrow h^+_{vb} + e^-_{cb} \quad (1)$$

$$S_2O_8^{2-} + e^-_{cb} \rightarrow SO_4\bullet^- + SO_4^{2-} \quad (2)$$

$$SO_4^{2-} + h^+_{vb} \rightarrow SO_4\bullet^- \quad (3)$$

wherein e^-_{cb} stands for photogenerated electrons in the conduction band and h^+_{vb} stands for photogenerated holes in the valence band. Owing to its higher nitrobenzene degradation efficiency, Ag (5%)/Pb_3O_4 was selected as a candidate for further testing.

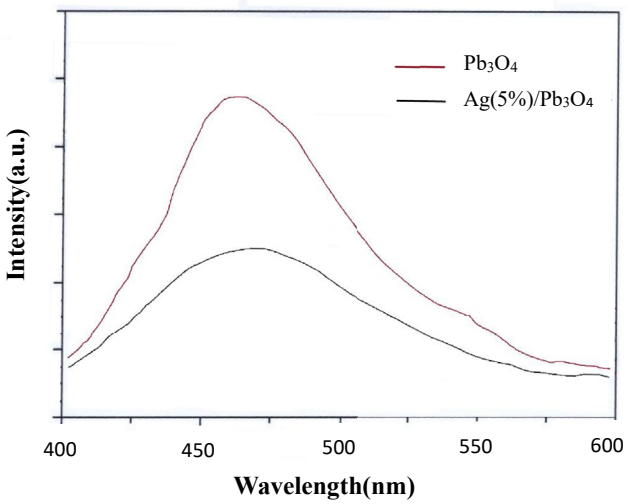

Figure 5. The photoluminescence spectra of Pb_3O_4 and Ag (5%)/Pb_3O_4 excited at 325 nm.

XPS measurements were executed for clarification of intrinsic electronic state of Ag (5%)/Pb_3O_4. Figure 1b presents the Pb 4f XPS spectra of original Ag (5%)/Pb_3O_4 and Ag (5%)/Pb_3O_4 reacted. As regards original Ag (5%)/Pb_3O_4 semiconductor, two peaks centered at 137.5 and 142.5 eV were found, which were assigned to the binding energy of Pb 4f $_{(7/2)}$ and Pb 4f $_{(5/2)}$, respectively (Kim et al., 1973; Morgan and Van Wazer, 1973; Thomas and Tricker, 1975). Nevertheless, the binding energy of Pb 4f $_{(7/2)}$ and Pb 4f $_{(5/2)}$ of Ag (5%)/Pb_3O_4 has shifted to 138.6 and 143.6 eV individually after execution of nitrobenzene oxidation. It clearly points out that Pb cations on the surface of Ag (5%)/Pb_3O_4 make deviation to higher oxidation states as compared with original one, in view of migration of photogenerated electrons to persulfate anions (Park et al., 2005; Zatsepin et al., 2017). The outcomes approve above supposition that persulfate anions could be directly activated by photogenerated electrons into sulfate radicals. Moreover, Ag (5%)/Pb_3O_4 may transform sulfate anions into sulfate radicals through the way of photogenerated

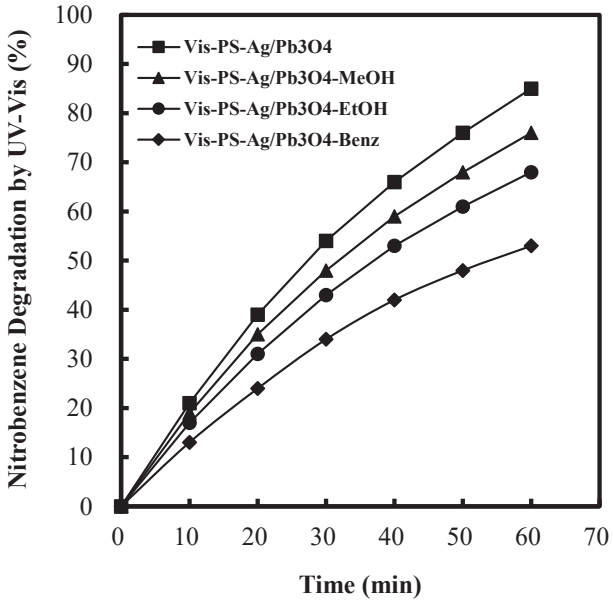

Figure 6. Effect of coexistence of benzene, ethanol and methanol respectively on the nitrobenzene removal percentage under the conditions of visible light power = 103.2 W, T = 318 K, persulfate concentration = 100 mM and Ag (5wt %)/Pb_3O_4 dosage = 1.5 g L^{-1}.

holes (Kanca and Uner, 2018). It provides other oxidants for nitrobenzene oxidation.

3.2. Physicochemical properties of Ag/Pb_3O_4

The XRD patterns of Ag/Pb_3O_4 semiconductors are demonstrated in Figure 2. Most peaks can be matched to crystal planes of Pb_3O_4 (Poll and Payne, 2015). The diffraction peak at 2θ values of 38.2° can be assigned to (111) plane of Ag metal (Anbu et al., 2019). It indicates that an insignificant amount of Ag metal was deposited on the surface of Pb_3O_4. Figure 3a illustrates the UV-vis diffuse reflectance spectra (DRS) of Ag/Pb_3O_4. The spectra of Ag/Pb_3O_4 and Pb_3O_4 exhibit similar strong absorbance band between the wavelength of 400 and 550 nm, which is at the visible light region. Especially, the absorbance intensity of Ag/Pb_3O_4 was higher than that of Pb_3O_4. It shows that Ag/Pb_3O_4 semiconductors are more sensitive to the visible light irradiation. The observation could be also attributed to Ag metal dopant, supplying an electron sink and inhibiting recombination of photogenerated electrons with holes on the surface of Pb_3O_4 (Han et al., 2012; Zhang et al., 2017). Further, the band gap energy of Ag/Pb_3O_4 was determined in accordance with the Tauc's equation $[(\alpha h\nu)^{1/n} = A\,(h\nu\text{-}E_g)]$, in which hν represented incident energy. The "n" value was set at the value of 1/2 based on the electronic transition state of semiconductors. The variation of $(\alpha h\nu)^2$ versus incident energy (hν) was plotted to procure the band gap energy by intercepting the tangent to the X-axis (Maji et al., 2011; Štengl and Grygar, 2011; Kamaraj et al., 2018). Thus, the band gap energy of Pb_3O_4 was estimated to be 2.20 eV, corresponding to the publication (Sharon et al., 1986). The band gap energy of a series of Ag/Pb_3O_4 semiconductors with Ag metal doped increasingly was determined to be 2.10, 2.01, 1.91, 1.82 and 1.72 eV, respectively (see Table 1). The superior photocatalytic behavior possessed by Ag (5%)/Pb_3O_4 could be interpreted with significant induced electron production, caused by lower band gap energy and more responsive to visible light irradiation. Apparently, the photo energy of visible light could excite Ag/Pb_3O_4 semiconductors to generate electron-hole pairs. Persulfate anions could be transformed into sulfate radicals by means of activation of photogenerated electrons, whereas photogenerated holes may convert sulfate anions into sulfate radicals simultaneously (see Eq. (2) and Eq. (3)).

FE-SEM images of Ag/Pb_3O_4 semiconductors are presented in Figure 3b. It clearly shows that the major surface of Pb_3O_4 was smooth. Instead, some irregularly shaped pellets deposited on Pb_3O_4 were observed referring to Pb_3O_4 doped with Ag metal. More clumps of pellets existed with increasing Ag loading. It seems that Ag metal was well dispersed on the surface of Pb_3O_4. The EDS element analyses on Ag/Pb_3O_4 semiconductors are presented in Figure 4. The weight percentages of Ag measured were consistent with those impregnated calculatedly (see Table 2). Figure 5 illustrates photoluminescence spectra of Pb_3O_4 and Ag (5%)/Pb_3O_4 excited at 325 nm. The main peak intensity of the latter was obviously lower than that of the former. It reveals that Ag (5%)/Pb_3O_4 exhibited lower recombination rate of photogenerated electron-hole pairs. The results support the issue of enhancement on photogenerated electrons of Pb_3O_4 by impregnation of Ag metal.

3.3. Effect of dosage of scavengers on persulfate integrated with Ag/Pb_3O_4 under visible light irradiation

Equals of benzene, ethanol and methanol respectively accompanied with nitrobenzene were agitated in wastewater to make clear reactive radicals originated from persulfate integrated with Ag/Pb_3O_4 under visible light irradiation. As illustrated in Figure 6, nitrobenzene removal percentages were seriously declined upon addition of benzene. The reaction rate constant between benzene and sulfate radicals has been estimated to be $3 \times 10^9\ M^{-1}\ s^{-1}$ (Liang and Su, 2009). Alternatively, ethanol and methanol input suppressed nitrobenzene abatement moderately. Ethanol and methanol reacted with sulfate radicals at the rate constants of $7.7 \times 10^7\ M^{-1}\ s^{-1}$ and $3.2 \times 10^6\ M^{-1}\ s^{-1}$ separately (Neta et al., 1988). Noticeably, the decay extent of nitrobenzene removal percentages agrees with the reactive trend among scavengers and sulfate radicals. It convinces us that sulfate radicals seem to be responsible for nitrobenzene oxidation in wastewater.

3.4. Effect of persulfate concentrations on persulfate integrated with Ag/Pb_3O_4 under visible light irradiation

The optimal persulfate concentration used is an important issue from an economic point of view. As given in Figure 7a, TOC removal percentages by a series of persulfate concentrations were presented in the time-flow mode. Apparently, the increment on persulfate concentrations raised nitrobenzene removal rates. As expected, high yields of sulfate

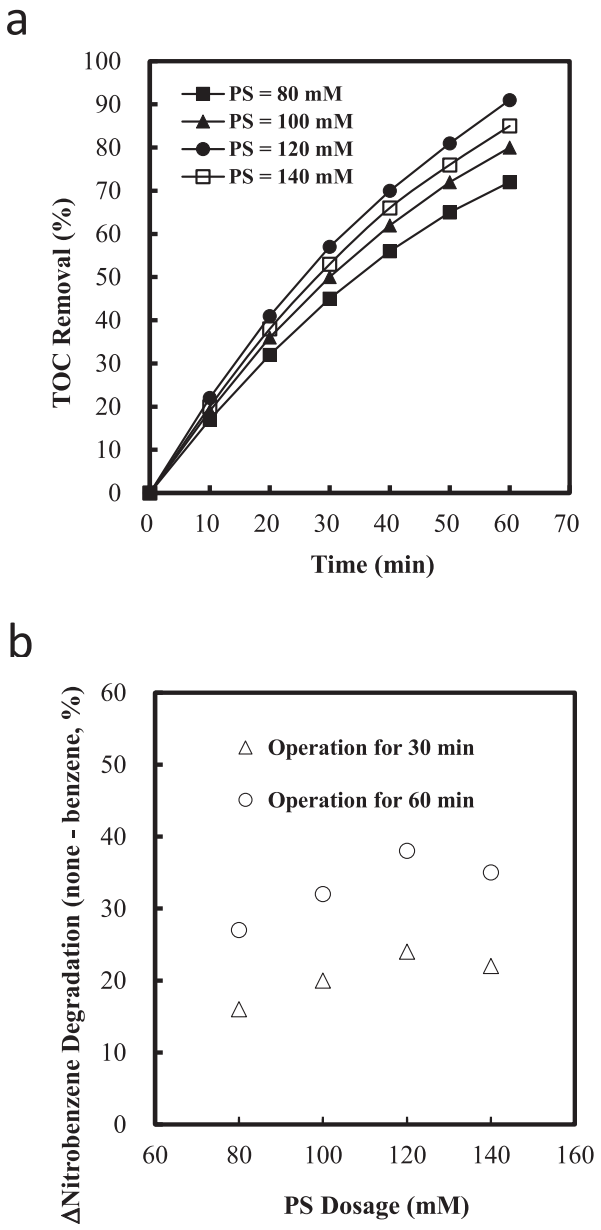

Figure 7. a Effect of persulfate concentrations on the TOC removal percentage under the conditions of visible light power = 103.2 W, T = 318 K and Ag (5wt %)/Pb_3O_4 dosage = 1.5 g L^{-1}. b The difference of nitrobenzene degradation percentage between the absence of benzene and presence of benzene under the conditions of visible light power = 103.2 W, T = 318 K and Ag (5wt%)/Pb_3O_4 dosage = 1.5 g L^{-1}, monitored by UV-Vis and served as scavenging effect.

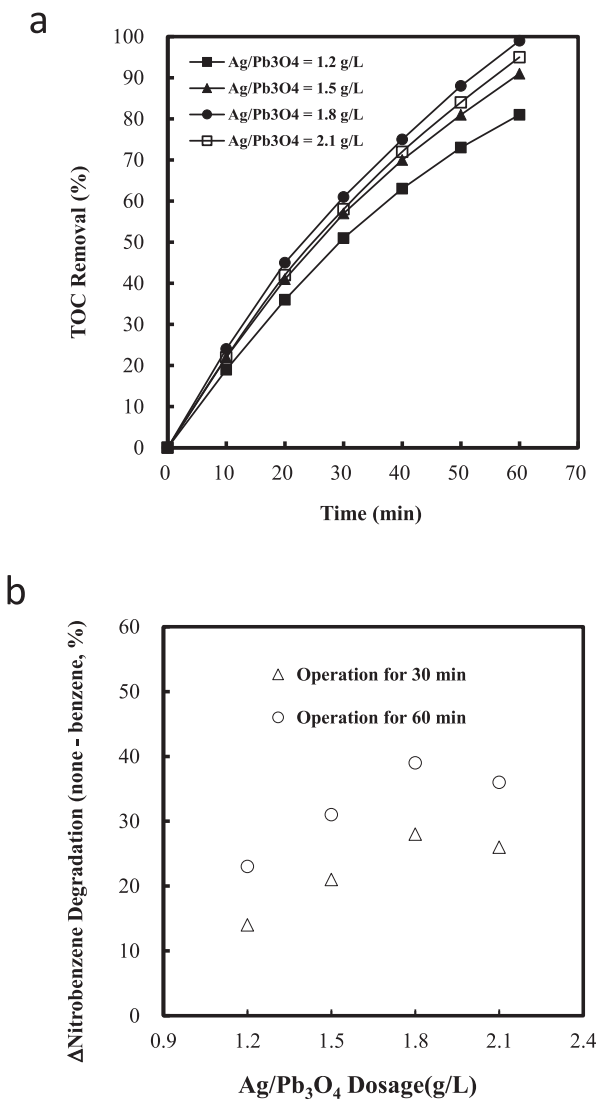

Figure 8. a Effect of Ag (5wt%)/Pb_3O_4 dosages on the TOC removal percentage under the conditions of visible light power = 103.2 W, T = 318 K and persulfate concentration = 120 mM. b The difference of nitrobenzene degradation percentage between the absence of benzene and presence of benzene under the conditions of visible light power = 103.2 W, T = 318 K and persulfate concentration = 120 mM, monitored by UV-Vis and served as scavenging effect.

radicals could be produced under the circumstance of high persulfate concentrations. However, the degradation efficiency of nitrobenzene was declined at the excess persulfate concentration (140 mM). The observation may be interpreted with happenings of unexpected reactions between sulfate radicals and overdosage of persulfate anions (Hou et al., 2012; Lin et al., 2013). Moreover, photocatalytic oxidation of nitrobenzene with the existence of benzene was carried out simultaneously to distinguish sulfate radicals yields by the scavenging effect (see Figure 7b). Surely, the scavenging effect monitors dramatically an analogous tendency with both sulfate radical yields and TOC removal modes. Thus, it supports that sulfate radicals were main oxidants.

3.5. Effect of Ag/Pb_3O_4 dosage on persulfate integrated with Ag/Pb_3O_4 under visible light irradiation

An optimal dosage of Ag/Pb_3O_4 semiconductor should be inevitably developed for promotion of nitrobenzene removal rate. The

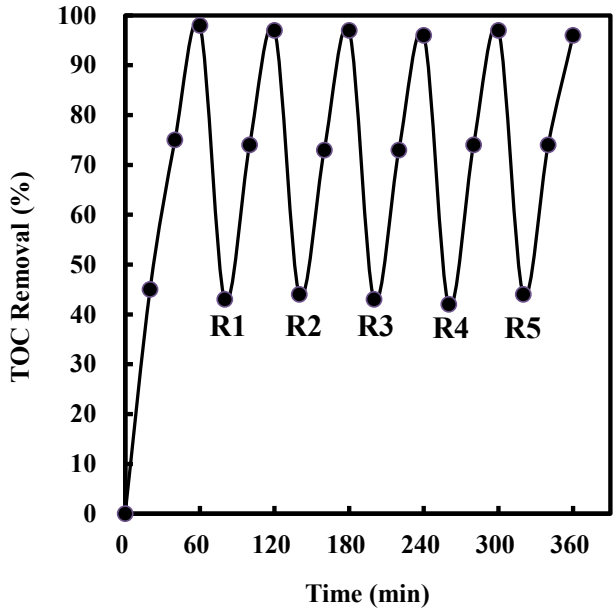

Figure 9. The photocatalytic stability of Ag (5wt%)/Pb_3O_4 examined by means of repetitions of five tests.

dosage effect referred to photocatalysis of Ag/Pb_3O_4 on persulfate activation was shown in Figure 8a. Naturally, TOC removal percentage increased with increasing dosages of Ag/Pb_3O_4, whereas it diminished for overdosage of Ag/Pb_3O_4 ($\geqq$ 2.1 g L^{-1}). The enhancement on the nitrobenzene decomposition rate may be interpreted with intense activation of persulfate anions by photocatalysis of Ag/Pb_3O_4, resulting in high yields of sulfate radicals. Nonetheless, visible light irradiation would be scattered and less semiconductors were exposed to the light on account of excessive dosage of Ag/Pb_3O_4 powder (Jyothi et al., 2014). Nitrobenzene degradation efficiency exhibited an identical trend as benzene scavenging effect (see Figure 8b). It implies that sulfate radicals were main oxidizing agents toward elimination of nitrobenzene. Particularly, the optimal conditions for overall oxidation of nitrobenzene within 60 min were found as follows: visible light power = 103.2 W, T = 318 K, persulfate concentration = 120 mM and Ag/Pb_3O_4 dosage = 1.8 g L^{-1}. In this study, the photocatalytic stability of Ag/Pb_3O_4 was examined by means of repetitions of five tests (shown in Figure 9). It clearly indicates that nitrobenzene removal efficiency reached to nearly 98% within the experiments. The results

Table 3. Compositions of feedstock and degradation intermediates identified by GC-MS.

Component	m/z (relative abundance, %)
Feedstock	
Nitrobenzene	50 (15.5), 51 (37.6), 65 (13.4), 74 (8.8), 77 (100), 78 (7.2), 93 (16.8), 123 (69.9), 124 (5.8)
Degradation intermediate	
2-Nitrophenol	39 (15.5), 53 (9.5), 63 (20.0), 64 (13.8), 65 (25.2), 81 (19.5), 93 (8.0), 109 (17.9), 139 (100)
3-Nitrophenol	38 (6.5), 39 (35.7), 53 (10.5), 63 (14.6), 64 (7.7), 65 (63.6), 81 (15.7), 93 (51.1), 139 (100)
4-Nitrophenol	39 (44.1), 53 (23.0), 62 (13.9), 63 (27.9), 65 (79.8), 81 (32.8), 93 (26.8), 109 (66.9), 139 (100)
Phenol	38 (5.0), 39 (12.3), 40 (6.8), 55 (6.2), 63 (6.3), 65 (20.7), 66 (27.1), 94 (100), 95 (7.5)
Hydroquinone	39 (6.8), 53 (14.2), 54 (12.7), 55 (10.4), 81 (25.2), 82 (12.0), 110 (100), 111 (5.9), 143 (9.4)
p-Benzoquinone	26 (17.9), 52 (17.7), 53 (17.0), 54 (63.1), 80 (28.1), 82 (36.0), 108 (100), 109 (8.0), 110 (11.9)

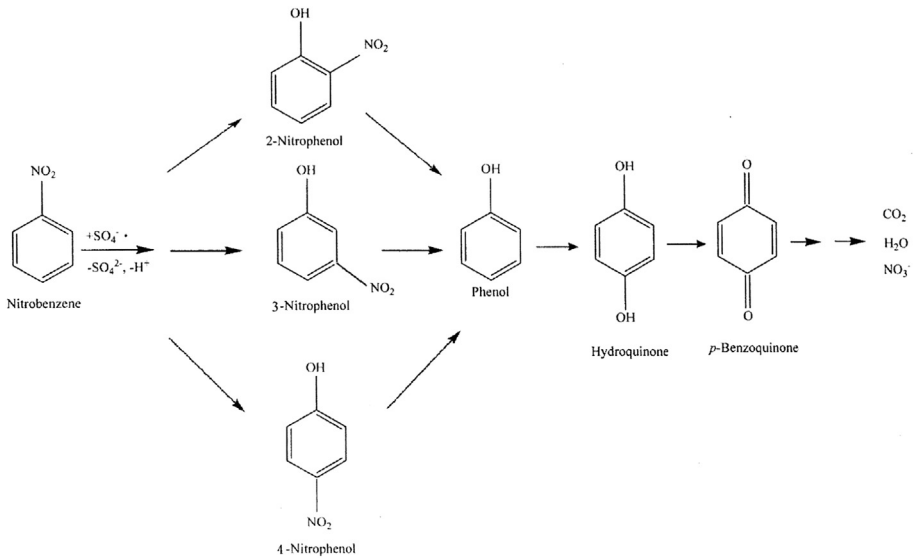

Figure 10. Plausible degradation pathways of nitrobenzene in wastewater by persulfate integrated with Ag/Pb_3O_4 under visible light irradiation.

convince us the feasibility of practical application of Ag/Pb_3O_4 for wastewater disposal.

3.6. Reaction pathways of nitrobenzene by persulfate integrated with Ag/Pb_3O_4 under visible light irradiation

All ingredients extracted from nitrobenzene oxidation using persulfate cooperated with Ag/Pb_3O_4 under visible light irradiation were analyzed through a GC-MS spectrometer. Table 3 summarizes the components acquired, including nitrobenzene feedstock, 2-nitrophenol, 3-nitrophenol, 4-nitrophenol, phenol, hydroquinone and *p*-benzoquinone. As far as 2-nitrophenol, 3-nitrophenol and 4-nitrophenol are concerned, they appear to be descended from hydroxycyclohexadienyl radicals, which execute O_2 addition and sequential HO_2• elimination to give hydroxylated products (Neta et al., 1988; Anipsitakis et al., 2006). It shows explicitly the occurrence of nitrophenol denitration due to detection on phenol (Zhou et al., 2015). Then, phenol was partially oxidized into hydroquinone, which would be successively transformed into *p*-benzoquinone by way of hydrogen abstraction. The ultimate products for nitrobenzene oxidation are composed of nitrate ions (sensed at UV-Vis 313 nm), carbon dioxide and water. In light of oxidative degradation intermediates authenticated, the probable pathways for nitrobenzene oxidation by persulfate integrated with Ag/Pb_3O_4 irradiated with visible light could be demonstrated in Figure 10.

4. Conclusions

According to previous discussion, nitrobenzene pollutants were predominantly mineralized by reactive sulfate radicals, originated from persulfate anions activated with photocatalysis of Ag/Pb_3O_4 semiconductors. It was strongly advocated through scavenging experiments, wherein nitrobenzene removal rates were suppressed sequentially by benzene, ethanol and methanol. In accordance with GC-MS analyses, the plausible degradation pathways for nitrobenzene oxidation are hypothesized as follows. Nitrobenzene was preliminarily converted into hydroxycyclohexadienyl radicals, which proceeded with subsequent oxidation to 2-nitrophenol, 3-nitrophenol and 4-nitrophenol, independently. Evidently, nitrophenol species were denitrated into phenol. Further oxidation of phenol gave rise to sequential synthesis of hydroquinone and *p*-benzoquinone. In the end, nitrobenzene would be completely mineralized into nitrate ions, carbon dioxide and water. The dramatic outcomes persuade us that persulfate combined with Ag/Pb_3O_4 under visible light irradiation is an effective manner for industrial wastewater treatment.

Declarations

Author contribution statement

Wen-Shing Chen: Conceived and designed the experiments; Performed the experiments; Analyzed and interpreted the data; Contributed reagents, materials, analysis tools or data; Wrote the paper.

Yi-Chen Liu: Conceived and designed the experiments; Performed the experiments; Analyzed and interpreted the data; Wrote the paper.

Funding statement

This research did not receive any specific grant from funding agencies in the public, commercial, or not-for-profit sectors.

Data availability statement

Data included in article/supp. material/referenced in article.

Declaration of interests statement

The authors declare no conflict of interest.

Additional information

No additional information is available for this paper.

References

Anbu, P., Gopinath, S.C.B., Yun, H.S., Lee, C.-G., 2019. Temperature-dependent green biosynthesis and characterization of silver nanoparticles using balloon flower plants and their antibacterial potential. J. Mol. Struct. 1177, 302–309.

Anipsitakis, G.P., Dionysiou, D.D., Gonzalez, M.A., 2006. Cobalt-mediated activation of peroxymonosulfate and sulfate radical attack on phenolic compounds Implications of chlorine ions. Environ. Sci. Technol. 40, 1000–1007.

Anotai, J., Sakulkittimasak, P., Boonrattanakij, N., Lu, M.C., 2009. Kinetics of nitrobenzene oxidation and iron crystallization in fluidized-bed Fenton process. J. Hazard Mater. 165, 874–880.

Carlos, L., Nichela, D., Triszcz, J.M., Felice, J.I., Einschlag, F.S.G., 2010. Nitration of nitrobenzene in Fenton's processes. Chemosphere 80, 340–345.

Chen, W.S., Huang, C.P., 2015. Mineralization of aniline in aqueous solution by electro-activated persulfate oxidation enhanced with ultrasound. Chem. Eng. J. 266, 279–288.

Chen, W.S., Huang, S.L., 2020. Photocatalytic degradation of bisphenol-A in aqueous solution by calcined PbO semiconductor irradiated with visible light. Desalination Water Treat. 190, 147–155.
Chen, Y., Li, H., Liu, W., Tu, Y., Zhang, Y., Han, W., Wang, L., 2014. Electrochemical degradation of nitrobenzene by anodic oxidation on the constructed TiO_2-NTs/SnO_2-Sb/PbO_2 electrode. Chemosphere 113, 48–55.
Chen, W.S., Shih, Y.C., 2020. Mineralization of aniline in aqueous solution by sono-activated peroxydisulfate enhanced with PbO semiconductor. Chemosphere 239, 124686.
Chen, C., Yan, X., Yoza, B.A., Zhou, T., Li, Y., Zhan, Y., Wang, Q., Li, Q.X., 2018. Efficiencies and mechanisms of ZSM5 zeolites loaded with cerium, iron, or manganese oxides for catalytic ozonation of nitrobenzene in water. Sci. Total Environ. 612, 1424–1432.
De Luca, A., He, X., Dionysiou, D.D., Dantas, R.F., Esplugas, S., 2017. Effects of bromide on the degradation of organic contaminants with UV and Fe^{2+} activated persulfate. Chem. Eng. J. 318, 206–213.
Duan, H., Liu, Y., Yin, X., Bai, J., Qi, J., 2016. Degradation of nitrobenzene by Fenton-like reaction in a H_2O_2/schwertmannite system. Chem. Eng. J. 283, 873–879.
Elshafei, G.M.S., Yehia, F.Z., Dimitry, O.I.H., Badawi, A.M., Eshaq, G., 2014. Ultrasonic assisted-Fenton-like degradation of nitrobenzene at neutral pH using nanosized oxide of Fe and Cu. Ultrason. Sonochem. 21, 1358–1365.
Gu, D., Dong, J., Zhang, Y., Zhu, L., Yan, C., Wu, H., Wang, B., 2018. An insight into pathways of solar-driven STEP oxidation of nitrobenzene by an integrated in situ thermoelectrochemical microreactor-analyzer. J. Clean. Prod. 200, 1026–1033.
Guo, J., Zhu, L., Sun, N., Lan, Y., 2017. Degradation of nitrobenzene by sodium persulfate activated with zero-valent zinc in the presence of low frequency ultrasound. J. Taiwan Inst. Chem. E. 78, 137–143.
Han, Z., Ren, L., Cui, Z., Chen, C., Pan, H., Chen, J., 2012. Ag/ZnO flower heterostructures as a visible-light driven photocatalyst via surface plasmon resonance. Appl. Catal. B Environ. 126, 298–305.
He, S.L., Wang, L.P., Zhang, J., Hou, M.F., 2009. Fenton pre-treatment of wastewater containing nitrobenzene using ORP for indicating the endpoint of reaction. Proc. Earth planet. Sci. 1, 1268–1274.
Holder, J.W., 1999. Nitrobenzene carcinogenicity in animals and human hazard evaluation. Toxicol. Ind. Health 15, 445–457.
Hou, L.W., Zhang, H., Xue, X.F., 2012. Ultrasound enhanced heterogeneous activation of peroxydisulfate by magnetite catalyst for the degradation of tetracycline in water. Sep. Purif. Technol. 84, 147–152.
Ji, Y., Shi, Y., Wang, L., Lu, J., 2017. Denitration and renitration processes in sulfate radical-mediated degradation of nitrobenzene. Chem. Eng. J. 315, 591–597.
Jiang, B.C., Lu, Z.Y., Liu, F.Q., Li, A.M., Dai, J.J., Xu, L., Chu, L.M., 2011. Inhibiting 1,3-dinitrobenzene formation in Fenton oxidation of nitrobenzene through a controllable reductive pretreatment with zero-valent iron. Chem. Eng. J. 174, 258–265.
Jyothi, K.P., Yesodharan, S., Yesodharan, E.P., 2014. Ultrasound (US), ultraviolet light (UV) and combination (US + UV) assisted semiconductor catalysed degradation of organic pollutants in water: oscillation in the concentration of hydrogen peroxide formed in situ. Ultrason. Sonochem. 21, 1787–1796.
Kamaraj, E., Somasundaram, S., Balasubramani, K., Eswaran, M.P., Muthuramalingam, R., Park, S., 2018. Facile fabrication of CuO-Pb_2O_3 nanophotocatalysts for efficient degradation of Rose Bengal dye under visible light irradiation. Appl. Surf. Sci. 433, 206–212.
Kanca, A., Uner, D., 2018. In situ and downstream sulfidation reactivity of PbO and ZnO during pyrolysis and hydrogenation of a high-sulfur lignite. Int. J. Hydrogen Energy.
Kim, K.S., O'Leary, T.J., Winograd, N., 1973. X-Ray photoelectron spectra of lead oxides. Anal. Chem. 45, 2214–2218.
Liang, C.J., Su, H.W., 2009. Identification of sulfate and hydroxyl radicals in thermally activated persulfate. Ind. Eng. Chem. Res. 48, 5558–5562.
Lin, H., Wu, J., Zhang, H., 2013. Degradation of bisphenol A in aqueous solution by a novel electro/Fe^{3+}/peroxydisulfate process. Sep. Purif. Technol. 117, 18–23.
Maji, S.K., Mukherjee, N., Dutta, A.K., Srivastava, D.N., Paul, P., Karmakar, B., Mondal, A., Adhikary, B., 2011. Deposition of nanocrystalline CuS thin film from a single precursor: structural, optical and electrical properties. Mater. Chem. Phys. 130, 392–397.
Mohammadikish, M., Zamani, K., 2018. Controlled construction of uniform pompon-like Pb-ICP microarchitectures as a precursor for PbO semiconductor nanoflakes. Adv. Powder Technol. 29, 2813–2821.
Morgan, W.E., Van Wazer, J.R., 1973. Binding energy shifts in the X-ray photoelectron spectra of a series of related group IV-A compounds. J. Phys. Chem. 77, 964–969.
Mukhopadhyay, I., Ghosh, S., Sharon, M., 1997. Surface modification by the potential delay technique to obtain a photoactive PbO film. Surf. Sci. 384, 234–239.
Neta, P., Huie, R.E., Ross, A.B., 1988. Rate constants for reactions of inorganic radicals in aqueous solution. J. Phys. Chem. Ref. Data 17, 1027–1284.
Nichela, D.A., Berkovic, A.M., Costante, M.R., Juliarena, M.P., Einschlag, F.S.G., 2013. Nitrobenzene degradation in Fenton-like systems using Cu(II) as catalyst. Comparison between Cu(II)- and Fe(III)-based systems. Chem. Eng. J. 228, 1148–1157.
Nitoi, I., Oancea, P., Raileanu, M., Crisan, M., Constantin, L., Cristea, I., 2015. UV-VIS photocatalytic degradation of nitrobenzene from water using heavy metal doped titania. J. Ind. Eng. Chem. 21, 677–682.
Pan, Y., Zhou, M., Li, X., Xu, L., Tang, Z., Sheng, X., Li, B., 2017. Highly efficient persulfate oxidation process activated with pre-magnetization Fe^0. Chem. Eng. J. 318, 50–56.
Park, C.H., Won, M.S., Oh, Y.H., Son, Y.G., 2005. An XPS study and electrical properties of $Pb_{1.1}Zr_{0.53}Ti_{0.47}O_3$/PbO/Si (MFIS) structures according to the substrate temperature of the PbO buffer layer. Appl. Surf. Sci. 252, 1988–1997.
Poll, C.G., Payne, D.J., 2015. Electrochemical synthesis of PbO_2, Pb_3O_4 and PbO films on a transparent conducting substrate. Electrochim. Acta 156, 283–288.
Qiao, J., Luo, S., Yang, P., Jiao, W., Liu, Y., 2019. Degradation of nitrobenzene-containing wastewater by ozone/persulfate oxidation process in a rotating packed bed. J. Taiwan Inst. Chem. E. 99, 1–8.
Ratanatamskul, C., Chintitanun, S., Masomboon, N., Lu, M.C., 2010. Inhibitory effect of inorganic ions on nitrobenzene oxidation by fluidized-bed Fenton process. J. Mol. Catal. A Chem. 331, 101–105.
Sakthivel, Y., Venugopal, G., Durairaj, A., Vasanthkumar, S., Huang, X., 2019. Utilization of the internal electric field in semiconductor photocatalysis: a short review. J. Ind. Eng. Chem. 72, 18–30.
Satdeve, N.S., Ugwekar, R.P., Bhanvase, B.A., 2019. Ultrasound assisted preparation and characterization of Ag supported on ZnO nanoparticles for visible light degradation of methylene blue dye. J. Mol. Liq. 291, 111313.
Sharon, M., Kumar, S., Jawalekar, S.R., 1986. Characterization of Pb_3O_4 films by electrochemical techniques. Bull. Mater. Sci. 8, 415–418.
Shen, X.Z., Liu, Z.C., Xie, S.M., Guo, J., 2009. Degradation of nitrobenzene using titania photocatalysts co-doped with nitrogen and cerium under visible light illumination. J. Hazard Mater. 162, 1193–1198.
Štengl, V., Grygar, T.M., 2011. The simplest way to Iodine-doped anatase for photocatalysts activated by visible light. Int. J. Photoenergy 2011, 685935–685948.
Sun, Y., Yang, Z., Tian, P., Sheng, Y., Xu, J., Han, Y.F., 2019. Oxidative degradation of nitrobenzene by a Fenton-like reaction with Fe-Cu bimetallic catalysts. Appl. Catal. B Environ. 244, 1–10.
Tayade, R.J., Bajaj, H.C., Jasra, R.V., 2011. Photocatalytic removal of organic contaminants from water exploiting tuned band gap photocatalysts. Desalination 275, 160–165.
Terpstra, H.J., De Groot, R.A., Haas, C., 1997. The electronic structure of the mixed valence compound Pb_3O_4. J. Phys. Chem. Solid. 58, 561–566.
Thomas, J.M., Tricker, M.J., 1975. Electronic structure of the oxides of lead: Part 2. - an XPS study of bulk rhombic PbO, tetragonal PbO, β-PbO_2 and Pb_3O_4. J. Chem. Soc., Faraday Trans. 2 Molecular and Chem. Phys. 71, 329–336.
Wang, G.X., Zhang, X.Y., Yao, C.Z., Tian, M.Z., 2011. Acute toxicity and mutagenesis of three metabolites mixture of nitrobenzene in mice. Toxicol. Ind. Health 27, 167–171.
Weavers, L.K., Liang, F.H., Hoffmann, M.R., 1998. Aromatic compound degradation in water using a combination of sonolysis and ozonolysis. Environ. Sci. Technol. 32, 2727–2733.
Weissermel, K., Arpe, H.-J., 1991. Ullmann's Encyclopedia of Industrial Chemistry, fifth ed., A17. VCH, Weinheim.
Xia, K., Xie, F., Ma, Y., 2014. Degradation of nitrobenzene in aqueous solution by dual-pulse ultrasound enhanced electrochemical process. Ultrason. Sonochem. 21, 549–553.
Zatsepin, D.A., Boukhvalov, D.W., Gavrilov, N.V., Zatsepin, A.F., Shur, V.Ya., Esin, A.A., Kim, S.S., Kurmaev, E.Z., 2017. Soft electronic structure modulation of surface (thin-film) and bulk (ceramics) morphologies of TiO_2-host by Pb-implantation: XPS-and-DFT characterization. Appl. Surf. Sci. 400, 110–117.
Zhang, X., Wang, Y., Hou, F., Li, H., Yang, Y., Zhang, X., Yang, Y., Wang, Y., 2017. Effects of Ag loading on structural and photocatalytic properties of flower-like ZnO microspheres. Appl. Surf. Sci. 391, 476–483.
Zhang, Y., Xu, X., Pan, Y., Xu, L., Zhou, M., 2019. Pre-magnetized Fe0 activated persulphate for the degradation of nitrobenzene in groundwater. Sep. Purif. Technol. 212, 555–562.
Zhang, Y., Zhang, K., Dai, C., Zhou, X., Si, H., 2014. An enhanced Fenton reaction catalyzed by natural heterogeneous pyrite for nitrobenzene degradation in an aqueous solution. Chem. Eng. J. 244, 438–445.
Zhao, L., Ma, W., Ma, J., Wen, G., Liu, Q., 2015. Relationship between acceleration of hydroxyl radical initiation and increase of multiple-ultrasonic field amount in the process of ultrasound catalytic ozonation for degradation of nitrobenzene in aqueous solution. Ultrason. Sonochem. 22, 198–204.
Zhao, L., Ma, J., Sun, Z.Z., Liu, H., 2009. Influencing mechanism of temperature on the degradation of nitrobenzene in aqueous solution by ceramic honeycomb catalytic ozonation. J. Hazard Mater. 167, 1119–1125.
Zhao, L., Ma, J., Sun, Z.Z., Zhai, X.D., 2008. Catalytic ozonation for the degradation of nitrobenzene in aqueous solution by ceramic honeycomb-supported manganese. Appl. Catal. B Environ. 83, 256–264.
Zhou, J., Xiao, J., Xiao, D., Guo, Y., Fang, C., Lou, X., Wang, Z., Liu, J., 2015. Transformations of chloro and nitro groups during the peroxymonosulfate-based oxidation of 4-chloro-2-nitrophenol. Chem. Eng. J. 134, 446–451.
Zhu, L., Ma, B., Zhang, L., 2007. The study of distribution and fate of nitrobenzene in a water/sediment microcosm. Chemosphere 69, 1579–1585.